Progress In Electromagnetics Research B, Vol. 47, 405–421, 2013

DESIGN OF TEMPLE SHAPE SLOT ANTENNA FOR ULTRA WIDEBAND APPLICATIONS

Raghupatruni V. Ram Krishna[1] and Raj Kumar[2, *]

[1]Research Scholar, DIAT (Deemed University), Girinagar, Pune 411 025, India

[2]ARDE, Pashan, Pune, India

Abstract—A novel design of a temple shaped printed slot antenna for circular polarization applications is presented in this paper. The slot, half trapezoidal and half semi-circular in shape, is excited by a 50 Ω CPW feed terminated with a tuning stub. Modifications of the initial design for improving return loss and circular polarization characteristics are proposed and discussed. The antenna is very compact (40 mm × 35 mm) in size and simple to design. The final version of the antenna offers an experimentally measured impedance bandwidth of 108%, i.e., from 2.75 GHz to 9.25 GHz. The 3-dB axial ratio bandwidth achieved is 51.6%, i.e., from 4.6 GHz to 7.8 GHz. The antenna is further characterized by a peak gain of about 5 dB and a relatively stable radiation pattern in the useful band.

1. INTRODUCTION

High data rate operating capability in a multipath fading environment and a large bandwidth capable of supporting several applications have become the prerequisites of any modern wireless communication system. Consequently, there is an ever increasing demand on the performance objectives of the printed antenna mostly used in such systems. In this regard, antennas supporting circular polarization (CP) and dual-polarization (DP) are being preferred and their properties being investigated by researchers around the world. Traditionally used in radar and satellite navigation applications where the receiver/transmitter orientation was unknown, CP antennas have been found to be effective in combating the destructive effects of multi-path fading and thus realizing high data transmission rates.

Received 10 November 2012, Accepted 9 January 2013, Scheduled 14 January 2013

* Corresponding author: Raj Kumar (raj34_shivani@yahoo.co.in).

Another recent application of CP antennas is for RFID systems where a continuously emitted rotating field has the capability of tagging any object on its way.

In principle, pure circular polarization is achieved when the generated electric field has two orthogonal modes with equal amplitude and 90 degree phase difference between them. The common techniques to achieve CP in a microstrip antenna include introduction of asymmetries in regular geometries, employing multiple feeds to achieve quadrature in space and time and deployment of additional parasitic patches intended to rotate the electric field vector [1]. CP antennas designed on microstrip patch structure suffered from low impedance bandwidth due to the inherent high quality (Q) factor. On the other hand, coplanar waveguide (CPW) feed besides giving a larger bandwidth allows for less dispersion, low radiation loss and good omni-directional radiation patterns with moderate gains. In addition, the absence of via-hole connections and small ground plane requirements ensure reduced cost and system complexity and facilitate easy integration with the adjacent radio frequency (RF) circuitry.

Several antenna configurations utilizing the CPW-feed in both the planar monopole form [2, 3] and printed slot form [4–11] have been reported in the literature, the latter having the additional advantage of a still wider bandwidth and increased degree of freedom for applying perturbations. A printed monopole antenna with a tuning stub shaped with one horizontal arm and one vertical arm was proposed in [2]. The CPW grounds were extended in the form of branches around the monopole and a useful (CP) bandwidth of about 20% was achieved around 5 GHz. In the monopole antenna discussed in [3], 8% axial ratio bandwidth (ARBW) was achieved from 2.21 GHz to 2.40 GHz. A hexagonal slot antenna with grounded inverted L-shaped strips attached to the slot and excited by a L-shaped monopole is investigated in [4] giving an AR bandwidth of about 50% (2.25 to 3.75 GHz). A 60×60 mm Printed Square Slot Antenna (PSSA) with E-shaped slits on the opposite corners of the ground plane and excited by a CPW-feed line was proposed in [5]. The 3 dB AR bandwidth achieved was 32.8% from 1810 MHz to 2520 MHz. In [6], a square slot having an inverted T-strip embedded to it and excited by a Halberd shaped feed line was proposed. The 3-dB ARBW achieved was 3.81% at 1.575 GHz. In [7], a square ground plane of size 60 mm $\times$ 40 mm with a circular slot excited by an equiangular tapered feedline was presented. The antenna achieved a very high axial ratio bandwidth (ARBW) about 61.9% (2.9 to 5.5 GHz). A stair shaped slot antenna with a CP bandwidth of 31.2% (2.30 to 3.15 GHz) was proposed in [8]. In [9], a square slot with a pair of inverted L grounded strips and excited by

a lightening shaped feed line was discussed. It was shown to achieve a CP bandwidth of 48.8% (2.075 GHz to 3.415 GHz). A printed square slot antenna (PSSA) excited by a halberd-shaped CPW feed line for circular polarization in the S-band was proposed in [10]. By placing an additional square ring patch in the slot center, the CP was obtained in the L-band as well. The CP bandwidth obtained was 29% in the L-band and 26% in the S-band. Another technique shown to achieve circular polarization in a square slot antenna was the employment of crooked T- and F-shaped strips suspended from the ground plane and protruding into the slot [11].

In this paper, a novel temple shaped printed slot antenna is proposed, the geometry of which is described in Section 2. The antenna is compact in size and useful for circular polarization applications in the WLAN (5–6 GHz) and WiMAX (7–8 GHz) and for other applications in the rest of the bandwidth. Three versions of the antenna were designed, optimized and tested using electromagnetic software: Ansoft HFSS based on the Finite Element Method (FEM) and CST Microwave Studio based on the Finite Integration Technique (FIT). The simulated results and behavioral analysis are discussed in Sections 3, 4 and 5. Also, a comparison of simulated results is made with the measured results of the fabricated prototypes.

2. ANTENNA CONFIGURATION

The design process is initiated by printing the ground plane on a substrate of dimensions $\mathbf{W} \times \mathbf{L}$ mm. Commercially cheap FR4 is used for the substrate which has a relative permittivity $\varepsilon_r = 4.4$ and a loss

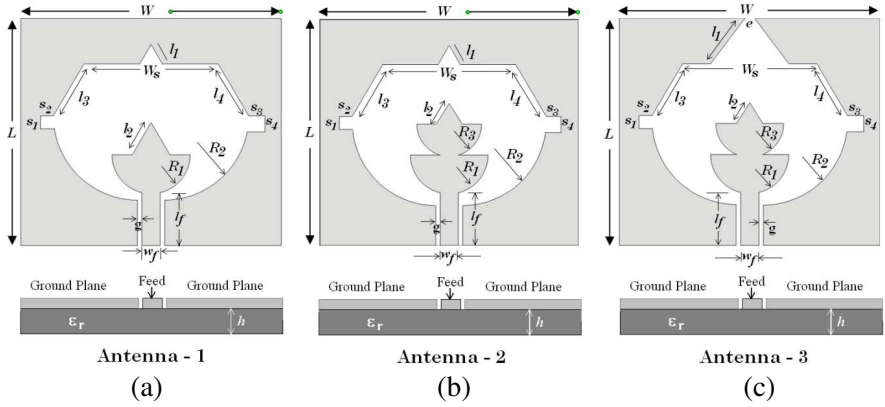

Figure 1. Configuration of the proposed antenna.

tangent of 0.02. The initial design is shown in Fig. 1(a). The slot etched on the ground plane resembles a trapezoid in the upper half and a semi-circle in the lower half. The semi-circle itself is formed by blending the adjacent corners of a rectangle using two circular arcs of radii R_2. The slot is excited by a 50 Ω CPW and to ensure maximum coupling, a semi-circular disc shaped tuning stub is attached to the end of the feed-line. For obtaining the desired CP characteristics, further perturbations in the form of rectangular and triangular stubs are added to the slot and the feedline.

To enhance the impedance and axial ratio bandwidths, the initial design is modified as suggested in Figs. 1(b) and 1(c). The modified versions are named Antenna-2 and Antenna-3. It can be seen from these figures that in version 2 of the antenna, the tuning stub incorporates an additional semi-circular disc of smaller radius R_3 while in the final version (the proposed antenna) the slot is opened at the top by a gap of dimension 'e'. The details of all the parameters for the three versions are indicated in Table 1.

3. SIMULATED AND EXPERIMENTAL RESULTS

Prototypes of Antenna-1 and Antenna-3 were fabricated with optimized dimensions and the reflection coefficient was measured using Rohde & Schwarz Vector Network Analyzer (ZVA-40). Figs. 2 and 3 show the photographs of the fabricated antennas and the compared reflection coefficient characteristics.

It is observed that there is a good agreement between the return losses simulated using CST and HFSS. A slight difference in the two simulated values is basically because of the two different numerical methods employed, i.e., FEM by the Ansoft HFSS and FIT by the CST Microwave Studio. A slight difference is also observed between

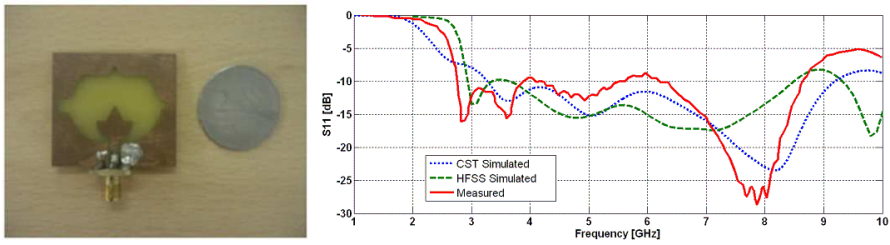

(a) (b)

Figure 2. (a) Photograph of the fabricated Antenna-1, (b) reflection coefficient (simulated & measured).

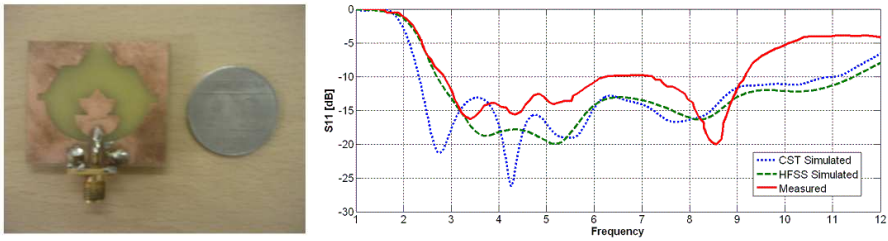

(a) (b)

Figure 3. (a) Photograph of the fabricated Antenna-3, (b) reflection coefficient (simulated & measured).

Table 1. Parameter details of the three antennas (all dimensions in mm).

Parameter	Antenna-1	Antenna-2	Antenna-3
W	40	40	40
L	35	35	35
$\mathbf{W_s}$	20.6	20.6	20.6
$\mathbf{l_1}$	3.46	3.46	8.75
$\mathbf{l_2}$	6.93	3.77	3.77
$\mathbf{l_3}$	9.3	9.3	9.3
$\mathbf{l_4}$	9.3	9.3	9.3
$\mathbf{R_1}$	6	6	6
$\mathbf{R_2}$	13	13	13
$\mathbf{R_3}$	–	5	5.2
$\mathbf{s_1}$	3	3	3
$\mathbf{s_2}$	2	2	2
$\mathbf{s_3}$	3	3	3
$\mathbf{s_4}$	3	3	2.5
e	–	–	1.5
$\mathbf{l_f}$	8	8	8
$\mathbf{w_f}$	2.8	2.8	2.8
g	0.7	0.7	0.7
h	1.53	1.53	1.53

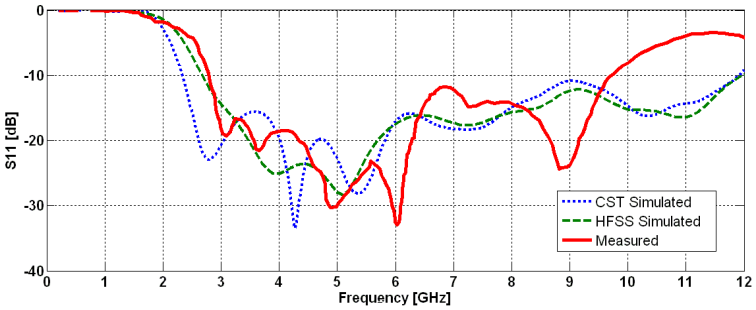

Figure 4. Simulated and measured reflection coefficient of Antenna-3A.

Table 2. Dimensions of Antenna-3A.

$\mathbf{W}$	$\mathbf{L}$	$\mathbf{W_s}$	$\mathbf{l_1}$	$\mathbf{l_2}$	$\mathbf{l_3}$	$\mathbf{l_4}$	$\mathbf{R_1}$	$\mathbf{R_2}$	$\mathbf{R_3}$
40	35	20.6	8.75	3.77	9.3	9.3	6.5	13	5.4
$\mathbf{s_1}$	$\mathbf{s_2}$	$\mathbf{s_3}$	$\mathbf{s_4}$	$\mathbf{e}$	$\mathbf{l_f}$	$\mathbf{w_f}$	$\mathbf{g}$	$\mathbf{H}$	
3	2	3	2.5	1.5	8	3.0	0.7	1.53	

the experimentally measured value of S_{11} and the simulated value. This is attributable to substrate variations over frequency, uncertainty in substrate thickness and dimensions of the 50 Ω connector used, fabrication tolerances and feed connector misalignment. It is also observed that the mismatch between the experimental and simulated reflection coefficient increases after 9 GHz which is due to the poor quality (frequency range) of the connector used. To further confirm this conclusion, a slight modification in some of the parameters of Antenna-3 was done to get a better S_{11} characteristic. The feed width $\mathbf{w}_f$ was increased from 2.8 mm to 3.0 mm and the radii of the semi-circular discs changed from $\mathbf{R}_1 = 6$ mm, $\mathbf{R}_3 = 5.2$ mm to $\mathbf{R}_1 = 6.5$ mm, $\mathbf{R}_3 = 5.4$ mm. With these dimensions, one more prototype (Antenna-3A) was fabricated and tested experimentally. The dimensional details of this antenna are given in Table 2 while the return loss characteristic (simulated and measured) is shown in Fig. 4 from which again the poor impedance matching with the connector is observed beyond 9 GHz.

4. COMPARISON OF THE THREE ANTENNAS

A comparison of the CST simulated performances of the three antennas (Antenna-1, Antenna-2 and Antenna-3) is presented here. The

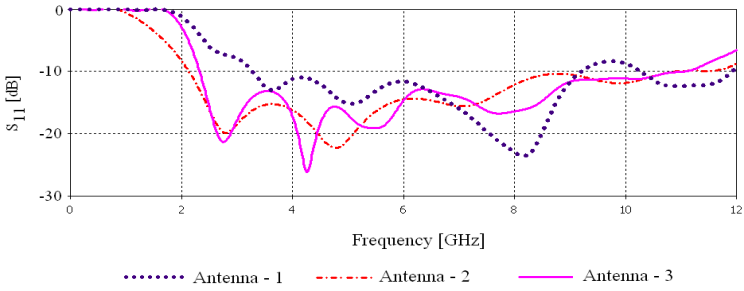

Figure 5. Simulated reflection coefficients of the three antennas.

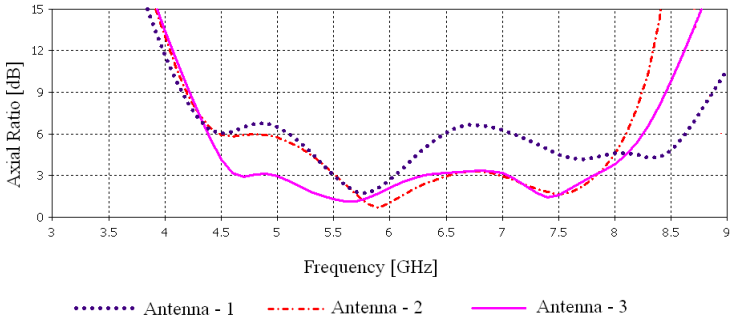

Figure 6. Simulated axial ratio of the three antennas.

Table 3. Performance statistics for the three versions.

	Return Loss		Axial Ratio	
	Range [GHz]	**BW [%]**	**Range [GHz]**	**BW [%]**
Antenna-1	3.2–9.2	96.77	5.5–6.1	10.34
Antenna-2	2.1–11	133.33	5.5–7.8	34.58
Antenna-2	2.3–11	130.83	4.6–7.8	51.61

reflection coefficient and the axial ratio are shown in Figs. 5 and 6, respectively.

It is clearly observed from Figs. 5 and 6 that an improvement in the 3-dB axial ratio and impedance bandwidth is obtained with successive modifications of the initial design. A brief statistics of the performance of the three designs is presented in Table 3.

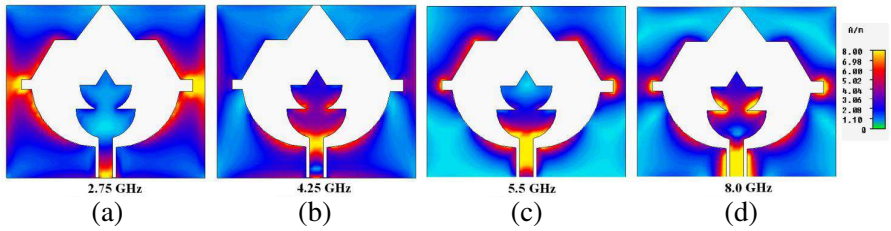

Figure 7. Surface current distribution for Antenna-3 at its resonant frequencies.

5. PERFORMANCE ANALYSIS

The return loss (RL) behavior of an ultra wideband antenna is usually described in terms of the resonant frequencies (dips) introduced due to perturbations, parasitic elements and harmonics. The overall broadband behavior of the antenna is obtained by the overlap of these resonant frequencies. Explanation for the resonant frequency obtained is usually decided by the feed structure employed. In particular, a CPW fed slot antenna is said to exhibit two modes of operation and correspondingly two distinct regions exhibiting resonance. The mode corresponding to the lower frequency is primarily determined by the dimensions of the slot antenna while the higher mode is set by the monopole like operation of the feed line [12, 13].

Considering the CST simulated RL characteristic of Antenna-3 (Fig. 5), we can note four dip resonances in the curve located at 2.75 GHz, 4.25 GHz, 5.5 GHz and 8 GHz. The surface current distribution at these resonant frequencies is shown in Fig. 7.

It can be seen that at 2.75 GHz, the current is mostly distributed around the slot periphery while the current distribution at 4.25 GHz is mostly found on the semi-circular shaped tuning stub validating the monopole like behavior of the antenna.

The dominant current paths corresponding to the first two resonant modes are shown in Figs. 8(a) and 8(b) respectively. The effective slot half perimeter as visualized from the current distribution (Fig. 7(a)) and obtained from the geometry (Fig. 8(a)) is given by

$$S_{hper} \sim \frac{\pi}{2} R_2 + S_1 + l_3 \tag{1}$$

this can then be made equal to half of the guided wavelength at the lower resonant frequency. Hence, the lower resonant frequency can be written as

$$f_1 = \frac{c}{2S_{hper}\sqrt{\epsilon_{r,eff}}} \tag{2}$$

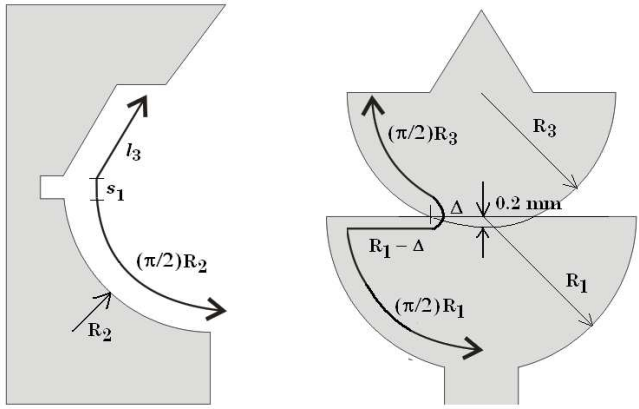

Figure 8. Current path for (a) the first and (b) the second resonant frequency.

The upper resonant frequency is obtained using

$$f_2 = \frac{c}{2h_s\sqrt{\epsilon_{r,eff}}} \tag{3}$$

where h_s is the effective stub length and from the geometry (Fig. 8(b)) is given by

$$h_s \sim \frac{\pi}{2}R_1 + \left(\frac{\pi}{2}R_3 - \Delta\right) + (R_1 - \Delta) \tag{4}$$

$$\Delta = \sqrt{R_3^2 - (R_3 - 0.2)^2} \tag{5}$$

In all the above expressions, 'c' stands for the velocity of light in free space, while $\varepsilon_{r,eff}$ is the effective relative permittivity of the substrate given by

$$\varepsilon_{r,eff} \approx \frac{\epsilon_r + 1}{2} \tag{6}$$

A comparison of the first two resonant frequencies calculated using (2) and (3) with the values obtained from simulation (CST) is shown in Table 4.

The current distribution at the third resonance, i.e., 5.5 GHz (Fig. 7(c)) shows a large number of minima (dips) around the slot periphery and the resonance obtained can be thought of as the second harmonic of the resonance at 2.75 GHz. Similarly, the resonance obtained at 8.0 GHz is the second harmonic of the resonance at 4.25 GHz. The increased current on the monopole edges at this

Table 4. Calculated and simulated resonant frequencies of Antenna-3.

	$\mathbf{S_{hper}}$ [mm]	$\mathbf{h_s}$ [mm]	$\varepsilon_{r,eff}$	Calculated Frequency (GHz)	Simulated Frequency (GHz)
$\mathbf{f_1}$	32.72	–	2.7	2.79	2.75
$\mathbf{f_2}$	–	22.28	2.7	4.10	4.25

frequency also leads to higher induced current around the rectangular stubs in the ground plane.

Another observation from the surface current plot is regarding the distribution of ground plane currents away from the slot periphery. It is seen that these currents are more evenly distributed at lower frequencies (2.75 GHz) as evident from the large bluish expanse, while at higher frequencies they approach the slot periphery due to increased monopole currents. This leads to the prospects of obtaining multiple polarization bands. The reduced currents away from the slot periphery at higher frequencies reduce the possibility of cross-polar cancellations at these frequencies and thus provide a better circular polarization characteristic (axial ratio).

5.1. CP Operation

The main objective of the antenna design was to realize good circular polarization characteristics. In this respect, perturbations in the form of triangular and rectangular stubs were added to the slot. Also, the tuning stub of the feedline was given appropriate modifications for achieving the desired behavior. As a result, the axial ratio bandwidth from CST MWS simulation is obtained from 4.6 GHz to 7.8 GHz (Fig. 9). The measured axial ratio and that computed using HFSS is also plotted alongside. The difference in the two axial ratios at the lower and upper limits is probably due to the differences in computational techniques used by the two software and the optimized dimensions for CST may differ from the optimized dimensions of HFSS.

The vector plot of the aperture electric field and surface current at one of the in-band frequencies (6 GHz) with increasing phase (at successive time instants) is shown in Fig. 10. From the figures, it can be seen that the electric field vector and so also the current vector undergo rotation with an advance in phase. Rotation is observable in both the clockwise and counter-clockwise directions explaining the presence of both left handed (LHCP) and right handed (RHCP) circular polarizations albeit in different quadrants.

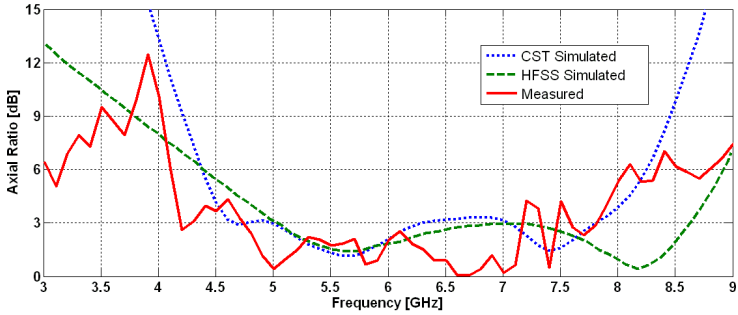

Figure 9. Axial ratio of Antenna-3.

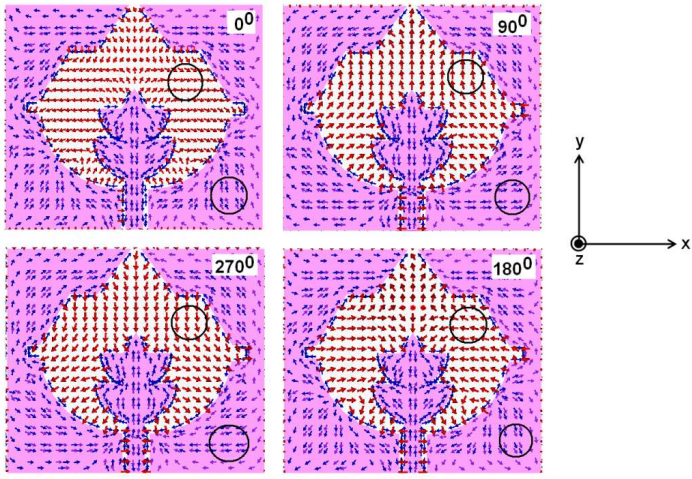

Figure 10. Aperture electric field and surface current at 6 GHz (Antenna-3).

Figure 11 shows the co polar (vertical) and cross polar (horizontal) component of the far field at 6 GHz. It also shows the LHCP/RHCP component at the same frequency. The high level of cross polarization (horizontal component) seen in Fig. 11 justifies the presence of circularly polarized behavior. Further, it can be seen that the electric field shows left handed CP above the $Z = 0$ plane ($\theta < 90°$, $\phi = 0°$) and a right handed CP below the $Z = 0$ plane ($\theta > 90°$, $\phi = 0°$).

The angular spread of circular polarization can be seen from the 2D Axial Ratio plot (simulated using CST MWS) as shown in Fig. 12. It is observed that CP characteristics dominate over much of the 3D space barring a small region (60° along ϕ) about bore sight.

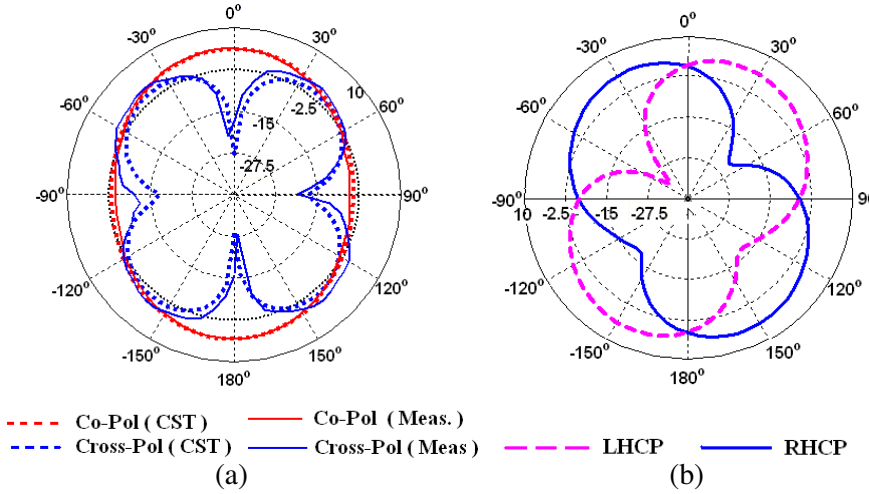

Figure 11. Co polar/cross polar plot and LHCP/RHCP plot at 6 GHz (H-Plane) for Antenna-3.

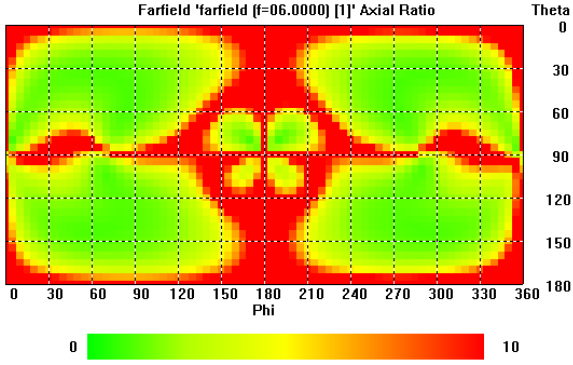

Figure 12. 2D axial ratio plot at 6 GHz (Antenna-3).

6. PARAMETRIC STUDY

The effects of varying the overall dimensions of the Antenna-3 are presented in this section. The slot and the stub dimensions remain unchanged in the study. The variations in the reflection coefficient magnitude and axial ratio with a change in the antenna length '**L**' and the width '**W**' are illustrated in Figs. 13 and 14, respectively.

It can be seen from Fig. 13 that the first two resonant frequencies slightly shift to the lower side with an increase in the length '**L**' of the

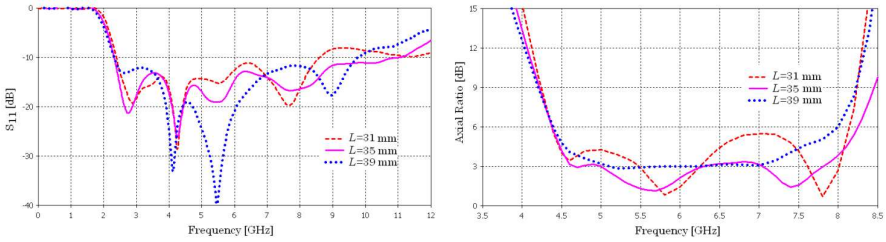

Figure 13. Effect of length '**L**' on the performance of antenna-3.

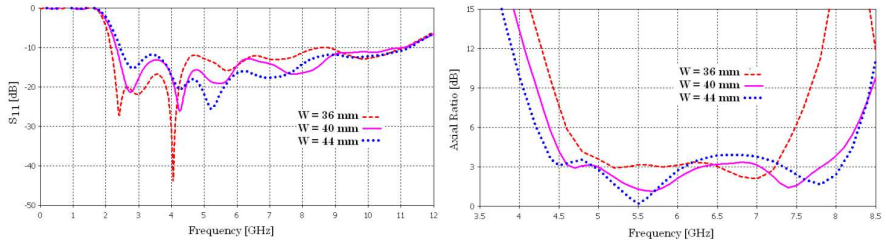

Figure 14. Effect of width '**W**' on the performance of Antenna-3.

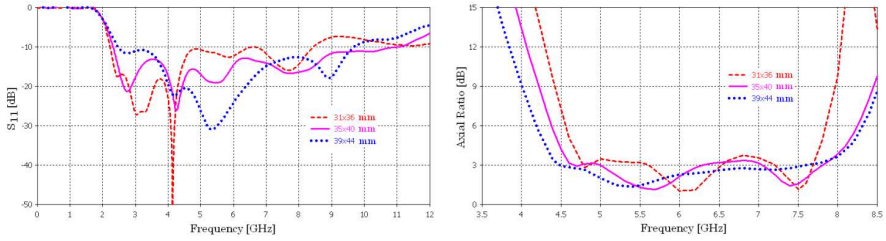

Figure 15. Effect of varying both '**L**' and '**W**' on the performance of Antenna-3.

antenna as expected. At the same time, the increase in '**L**' strengthens the vertical component deteriorating the axial ratio near the resonant frequency. An increase in the width '**W**' relaxes the enforcement of current around the slot periphery causing a slight decrease in the current path accompanied by a consequent increase in the first resonant frequency (Fig. 14). Also it is seen that the cross-polar component increases leading to a better axial ratio near the resonant frequency.

Figure 15 shows the effect of increasing both the length '**L**' and the width '**W**" (keeping the aspect ratio to be same) on the antenna performance. There is a better impedance matching at lower

frequencies for smaller size while for larger antennas; the axial ratio improves due to increased cross-polarization. It can be concluded from the study, that an optimized value of '**L**" and '**W**' give the best performance in terms of good return loss and axial ratio characteristics.

7. RADIATION PATTERNS, GAIN AND EFFICIENCY

The E-Plane and H-Plane radiation patterns of Antenna-3 have been calculated by using the electromagnetic solvers CST Microwave Studio and HFSS at the selected frequencies of 4 GHz, 6 GHz and 8 GHz. The radiation patterns were also measured in the in-house anechoic chamber at the same frequencies. The simulated and measured patterns are shown in Figs. 16 and 17, respectively.

Nature of the radiation patterns in the H-plane is nearly omni-directional while in the E-plane the radiation patterns follow the figure

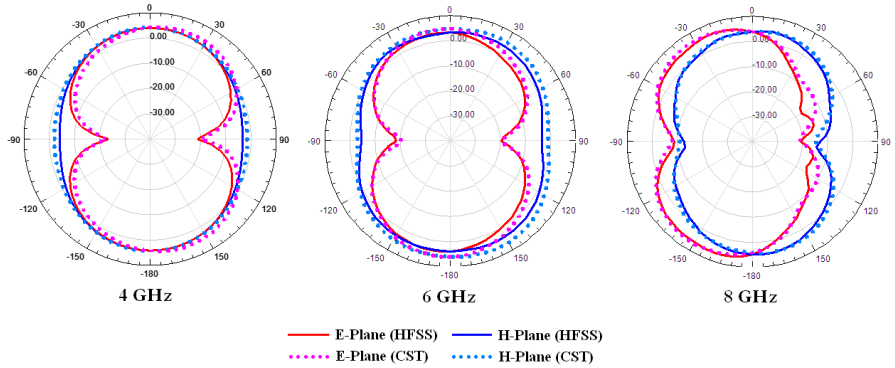

Figure 16. Simulated radiation patterns of Antenna-3 at 4 GHz, 6 GHz and 8 GHz.

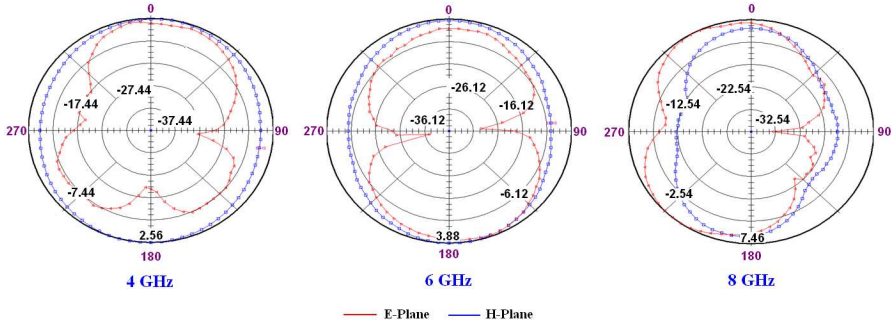

Figure 17. Measured radiation patterns of Antenna-3 at 4 GHz, 6 GHz and 8 GHz.

of eight. There is a slight distortion in the radiation pattern at higher frequency due to the unequal phase distribution of the aperture electric field and increase in the magnitude of higher order modes. It can be seen that the radiation patterns calculated by both the software are very close to each other.

A plot of the measured and simulated peak gain is shown in Fig. 18 while the gain along the boresight direction is shown in Fig. 19. The simulated radiation efficiency is presented in Fig. 20. The peak gain remains between 4 to 5 dB in the useful band while showing an increase in the high frequency region which is due to the increased effective area of the antenna at shorter wavelengths. A dip in the peak gain is seen at around 9.5 GHz which can be because of the return loss at this frequency and it is also reflected in the radiation efficiency (Fig. 19). The measured gain which includes the losses, drops after 9 GHz due to poor connector performance as also seen in the reflection coefficient characteristic of Antenna-3 (Fig. 3(b)). The radiation efficiency as calculated by CST Microwave Studio is seen to be slightly lesser than that obtained using HFSS.

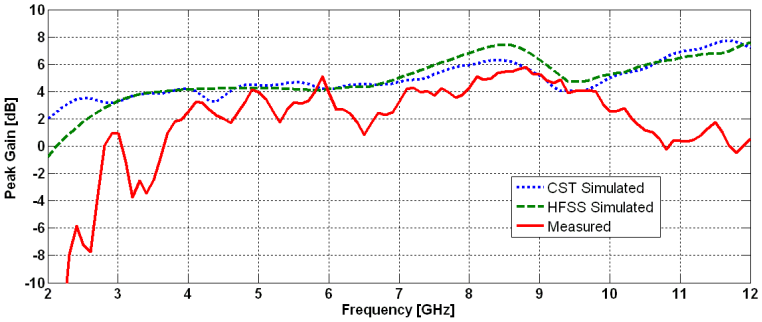

Figure 18. Simulated & measured peak gain of Antenna-3.

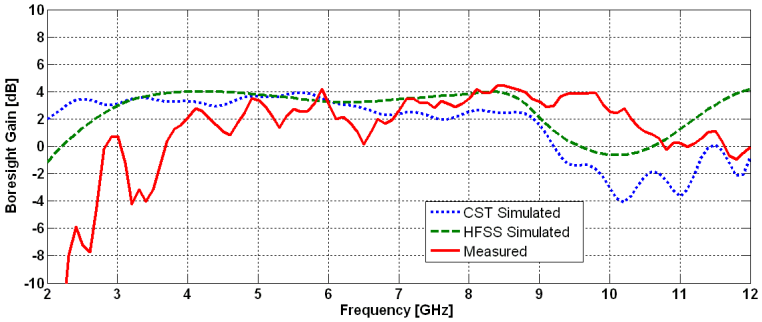

Figure 19. Simulated & measured boresight gain of Antenna-3.

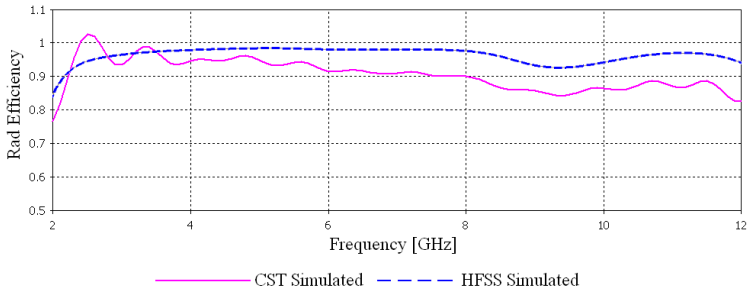

Figure 20. Simulated radiation efficiency of Antenna-3.

8. CONCLUSION

A compact CPW-fed temple shaped slot antenna with good circular polarization characteristics has been designed and validated. The modified versions of the initial design of the antenna offer improvement in axial ratio and impedance bandwidths. The proposed antenna offers an impedance bandwidth of about 108% (2.75 GHz–9.25 GHz) and an axial ratio bandwidth of about 52% (4.6 GHz–7.8 GHz). The peak gain remains around 5 dB in the useful band. A brief analysis of the performance was also discussed. The antenna can be used in the circular polarization band for WLAN and WiMAX and for applications like military imaging and vehicular radar with vertical polarization in the remaining band.

ACKNOWLEDGMENT

The authors thank the reviewers for their comments and valuable suggestions. The first author is a research fellow at the Defence Institute of Advanced Technology (Deemed University), Pune, India and acknowledges the financial support and facilities extended for carrying out the research work.

REFERENCES

1. Lee, K. F. and K. M. Luk, *Microstrip Patch Antennas*, Imperial College Press, London, UK, 2011.
2. Chang, T. N. and G. A. Tsai, "A wideband coplanar waveguide-fed circularly polarized antenna," *IET Microwaves and Antennas Propagation*, Vol. 2, No. 4, 343–347, 2008.

3. Augustin, G. and T. A. Denidni, "Coplanar waveguide-fed uniplanar trapezoidal antenna with linear and circular polarization," *IEEE Transactions on Antennas and Propagation*, Vol. 60, No. 5, 2522–2526, May 2012.
4. Zhou, S.-W., P.-H. Li, Y. Wang, W.-H. Feng, and Z.-Q. Liu, "A CPW-fed broadband circularly polarized regular-hexagonal slot antenna with L-shape monopole," *IEEE Antennas and Wireless Propagation Letters*, Vol. 10, 1182–1185, 2011.
5. Du, S. and Q.-X. Chu, "A CPW-fed broadband circularly-polarized square slot antenna with E-shaped slits in ground plane," *Proceedings of the 39th European Microwave Conference*, 225–227, Rome, Italy, 2009.
6. Sze, J.-Y. and S.-P. Pan, "Design of CPW-fed circularly polarized slot antenna with a miniature configuration," *IEEE Antennas and Wireless Propagation Letters*, Vol. 10, 1465–1468, 2011.
7. Chen, Q., H.-L. Zheng, T. Quan, and X. Li, "Broadband CPW-fed circularly polarized antenna with equiangular tapered-shaped feedline for ultra-wideband applications," *Progress In Electromagnetics Research C*, Vol. 26, 83–95, 2012.
8. Wang, C.-J. and C.-H. Chen, "CPW-fed stair-shaped slot antennas with circular polarization," *IEEE Transactions on Antennas and Propagation*, Vol. 57, No. 8, 2483–2486, August 2009.
9. Sze, J.-Y., C.-I. G. Hsu, Z.-W. Chen, and C.-C. Chang, "Broadband CPW-fed circularly polarized square slot antenna with lightening-shaped feedline and inverted-L grounded strips," *IEEE Transactions on Antennas and Propagation*, Vol. 58, No. 3, 973–977, March 2010.
10. Sze, J.-Y. and S.-P. Pan, "Design of broadband circularly polarized square slot antenna with compact size," *Progress In Electromagnetics Research*, Vol. 120, 513–533, 2012.
11. Ahdi Rezaeieh, S. and M. Kartal, "A new triple band circularly polarized square slot antenna design with crooked T- and F-shaped strips for wireless communications," *Progress In Electromagnetics Research*, Vol. 121, 1–18, 2011.
12. Chen, W. S., "A novel broadband design of a printed rectangular slot antenna for wireless applications," *Microwave Journal*, Vol. 49, No. 1, 122–130, 2006.
13. Li, P., J. Liang, and X. Chen, "Study of printed elliptical/circular slot antennas for ultrawideband applications," *IEEE Transactions on Antennas and Propagation*, Vol. 54, No. 6, 1670–1675, 2006.